Time-dependent Boltzmann kinetic model of x rays produced by ultrashort-pulse laser irradiation of argon clusters

J. Abdallah, Jr. and G. Csanak
Theoretical Division, Los Alamos National Laboratory, Los Alamos, New Mexico 87545, USA

Y. Fukuda, Y. Akahane, M. Aoyama, N. Inoue, H. Ueda, and K. Yamakawa
Advanced Photon Research Center, Japan Atomic Energy Research Institute (JAERI), 8-1 Umemidai, Kizu-cho, Souraku-gun, Kyoto 619-0215, Japan

A. Ya. Faenov, A. I. Magunov, T. A. Pikuz, and I. Yu. Skobelev
Multicharged Ions Spectra Data Center of VNIIFTRI, Mendeleevo, Moscow Region 141570, Russia
(Received 18 July 2003; published 12 December 2003)

The Boltzmann equation and a detailed collisional-radiative model are solved simultaneously as a function of time to model the time-integrated x-ray spectra of the transient plasma produced by a high intensity ultrafast laser source. Level populations are calculated by solving the rate equations as a function of time using rate coefficients corresponding to a time varying electron energy distribution function (EEDF) determined by the solution to the Boltzmann equation. Electron-electron interactions are included through the solution of the Fokker-Planck equation. It is assumed that all the ions are initially in the Ne-like ground state due to the laser prepulse and that all free electrons have high energy (5 keV) from the fast laser deposition. The collisional-radiative model included over 3000 levels in the Ne-like through H-like ion stages of argon. The results are in agreement with highly resolved F-like to He-like *K*-shell emission spectra recorded recently during ultrashort laser experiments with argon cluster targets in Japan. The calculated time scale for emission is consistent with estimates of cluster decay times for these conditions. The calculations also show that the typical Li-like and Be-like satellite structure, sometimes attributed to a hot-electron component in the EEDF, can also be due to transient effects in a high-temperature ionizing plasma.

DOI: 10.1103/PhysRevA.68.063201 PACS number(s): 36.40.Vz, 52.50.Jm, 52.70.La

I. INTRODUCTION

The use of clusters as targets for high-power ultrashort laser pulses has been the subject of much research in recent years [1–29]. Cluster targets absorb laser pulse energy more efficiently than the corresponding gas and thus provide the capability to create high density plasmas [13,19] from these atoms. Also, cluster targets can be more effective than solid targets because of decreased energy loss due to conduction. Cluster targets have been suggested as sources of x rays for various purposes and the possibility for obtaining nuclear fusion [4,30,31] with them is also being investigated.

Until recently, most attempts to model the x-ray emission spectra observed from these experiments have used stationary-state kinetics with a prescribed temperature and density, and sometimes a provision for energetic electrons [10–13,18–23,25] has been included. In the present work, a combination of the Boltzmann equation and atomic kinetics rate equations are used to model the level populations of argon as a function of time, from the highly nonequilibrium state when the laser energy is deposited on a femtosecond time scale into hot electrons, until several picoseconds later when the plasma electrons relax and thermalize to a equilibrium Maxwellian distribution. During this time period the plasma is transient and not steady state, and the electron distribution can be non-Maxwellian for some time. The ionization state starts out underionized compared to the amount of electron energy available, and hence, ionization, excitation, and x-ray emission proceed until the plasma clusters expand and cool.

To the best of our knowledge, this is the most detailed calculation of the spectroscopic properties of a plasma using nonequilibrium electron energy distribution functions (EEDF's) obtained from the Boltzmann equation. The calculations solve for the distribution of 100 electron energy bins simultaneously with the populations of over 3000 levels from Ne-like to H-like argon. The calculations took 215 h of CPU time on a single processor of an SGI Origin 200 computer.

II. EXPERIMENTAL METHOD

The Ar cluster experiments were performed with the JAERI (Kyoto, Japan) 100 TW Ti:sapphire laser system based on the technique of chirped pulse amplification, which was designed to generate 20 fs pulses at a 10 Hz repetition rate and capable of producing focusing intensity up to 10^{20} W/cm^2 [32,33]. The laser pulses centered at 800 nm were generated at 82.7 MHz by a Ti:sapphire laser oscillator (10 fs). The pulses from the oscillator were stretched to 10 ns, and amplified by a regenerative amplifier and two stages of a multipass amplifier. In this study the amplified pulses were compressed to 30 fs by a vacuum pulse compressor yielding a maximum pulse energy of 360 mJ. In this system, after the regenerative amplifier, the pulses go through two double Pockels cells to reduce the prepulse. The contrast ratio between the main pulse and the prepulse that precedes

it by 1 ns is greater than $10^5:1$.

In a vacuum target chamber, the compressed pulses were introduced by a pair of Au-coated plane mirrors and focused by an f/3 Au-coated off-axis parabolic mirror. The measured spot size was 11 μm at $1/e^2$, which was 1.1 times as large as that of the diffraction limit. Approximately 64% of the laser energy was contained in the 11-μm Gaussian spot. These parameters give a focused laser peak intensity of 1.0×10^{19} W/cm^2 with a pulse duration of 30 fs and a pulse energy of 200 mJ.

Ar clusters were produced by expanding high-pressure (6 MPa) Ar gas into vacuum through a specially designed pulsed conical nozzle; the input and output diameters of the nozzle were 0.5 and 2.0 mm, respectively, and its length was 75 mm. The parameters of cluster targets were calculated using the code developed at the Institute for Mathematical Modeling, Russian Academy of Sciences [18,34,35]. By using this nozzle, we could produce Ar clusters with an average diameter of about 1 μm. The laser was focused about 1.5 mm below the nozzle.

The spatially resolved x-ray spectra were measured using focusing spectrometers with spatial resolution [36–39]. This spectrometer is equipped with a spherically bent mica crystal ($R=150$ mm) and a vacuum compatible x-ray change-coupled device camera (DX420-BN, AN-DOR). The spherically bent crystal was placed at a distance of 381.2 mm from the plasma source and was centered at $\lambda=4.05$ Å, which corresponds to a Bragg angle of 35.7° for fourth-order reflection of the crystal. The spectrometer was oriented in such a way that it was possible to obtain spatial resolution in the direction perpendicular to laser propagation. The measured size of the emission zone in this direction was less than 200 μm for obtaining the He-like α and β spectrum of Ar including the associated dielectronic satellite lines.

III. THEORETICAL METHOD

The details of the simulation approach are presented in this section. The basic method developed by Bretagne *et al.* [40] is used to propagate the EEDF in time. The method has previously been used to study the gas response to high-energy electron-beam injection [41]. A bin representation for the EEDF is introduced, i.e.,

$$f(E,t)=f(E_i,t),\quad E_i-\frac{\Delta E}{2}\leqslant E<E_i+\frac{\Delta E}{2},$$

$$i=1,\ldots,N_b, \tag{1}$$

where E is electron energy, f is the EEDF (the number of free electrons per unit energy interval per unit volume), and N_b is the total number of bins used, E_i is the energy associated with bin i, and ΔE is the bin size. In this case the Boltzmann equation reduces to a system of coupled first-order differential equations, which should ideally include all collision processes capable of altering individual electron energies:

$$\frac{df_i}{dt}=S_i(\mathbf{f},\mathbf{N}),\quad i=1,\ldots,N_b, \tag{2}$$

where $f_i=f(E_i,t)$, $\mathbf{f}$ represents all the components of f_i, and $\mathbf{N}$ corresponds to the set of population densities of levels included in the collisional-radiative model. The differential equation for the EEDF used here contains terms that include both elastic electron-electron collisions and inelastic collisions and is represented by the functional S in the above equation. The inelastic terms are expressed in standard form, each is given in terms of the level population densities, the appropriate cross section and the bin dependent EEDF.

The elastic electron-electron contribution was evaluated using the Fokker-Planck equation with the standard Rosenbluth potential [42] (this is the small momentum-transfer approximation for the description of the collision of a charged particle with all the other charged particles in the plasma). The inelastic processes include electron-impact excitation that reduces the energy of the incoming electron by the transition energy, electron-impact deexcitation that increases the energy of the incoming electron by the transition energy, and electron-impact ionization that reduces the electron energy by the ionization potential and creates a new free electron. The differential ionization cross section [43] was used to estimate the energy probability of both the final-state primary and secondary (ionized) electrons.

The population densities are given by the time dependent solution of the rate equations

$$\frac{dN_j}{dt}=R_j(\mathbf{f},\mathbf{N}),\quad j=1,\ldots,M, \tag{3}$$

where N_j is an individual component of $\mathbf{N}$, M is the number of levels included in the collisional-radiative model, and all population altering processes are represented through the functional R. The dependence of the right-hand side of Eq. (3) on $\mathbf{f}$ occurs through rate coefficients that are obtained by integrating the various cross sections over the EEDF. The total ion density is assumed to be constant as a function of time, thus neglecting the hydrodynamics of cluster expansion. The collisional-radiative model for argon was used previously for the interpretation of plasma focus experiments [44]. The model includes over 3000 fine-structure levels over the Ne-like through H-like ionization states. The atomic configurations were truncated at principal quantum number $n=3$ to limit the number of levels produced. The atomic data also features all the possible $n=1$ to $n=2$ x-ray transitions within the $n=3$ manifold for spectral comparison purposes.

The integration time span is divided into intervals. The initial level populations are held constant during the interval to propagate the EEDF from the beginning to the end of the interval using Eq. (2). Then the calculated EEDF is used to propagate the initial level populations via Eq. (3) to the end of the interval. This separation is possible because the level populations vary slowly compared to the EEDF. This procedure results in a significant saving in computer time since the level kinetics need not be calculated on the same time scale as the EEDF. The accuracy was tested by decreasing the interval size and checking the results. The procedure is re-

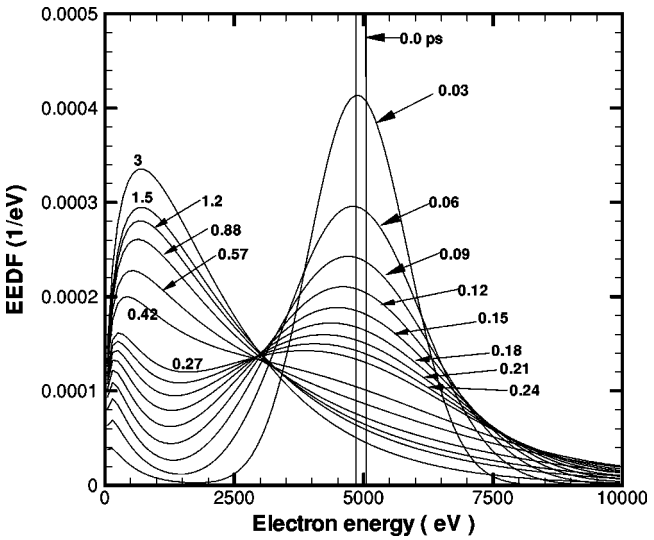

FIG. 1. The calculated EEDF as a function of electron energy (eV) for various times from 0 to 3 ps.

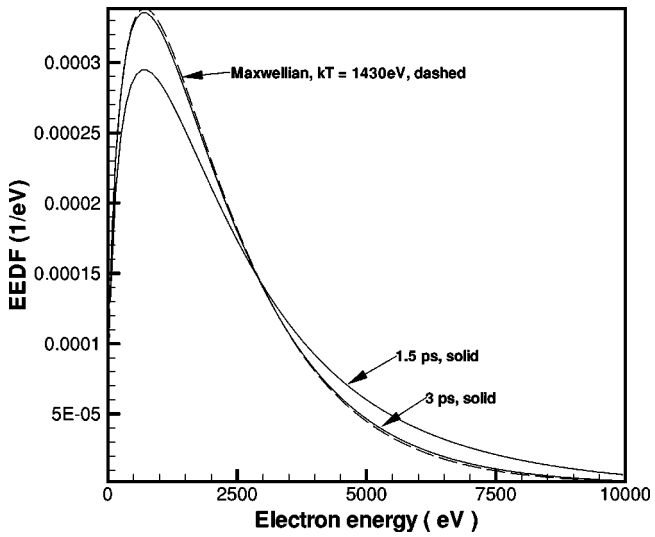

FIG. 2. The calculated EEDF at 1.5 and 3 ps compared to a Maxwellian distribution evaluated at 1430 eV.

peated over the entire time span of interest. The level populations are collected as a function of time and are used to calculate a time-integrated line emission spectrum. Gaussian line shapes with widths corresponding to approximately the instrumental resolution, $\lambda/\Delta(\lambda)=0.0006$, were employed.

Specifically, for the model calculations considered here, the atom number density was taken to be 6×10^{20} cm^{-3}, and initially all the ions were assumed to be in the ground state of the Ne-like ion. Thus, by charge neutrality, the initial electron density was 4.8×10^{21} cm^{-3}. The initial ionization state was chosen to be a rough approximation of the plasma condition after irradiation by the laser prepulse. This is a reasonable assumption because the Ne-like ionization state is dominant over a large range of temperature because of its relatively high ionization potential. The density was chosen to roughly correspond to the observed resonance to intercombination line ratio. The EEDF was divided into 100 equally spaced bins from 0 to 10 keV. For the initial EEDF, all the free electrons were placed in the bin near 5 keV for convenience. This choice is quite artificial but represents the extreme case of a completely non-Maxwellian initial EEDF with hot electrons. The 5 keV starting energy was also chosen to be in the center of the bin system for numerical stability. One hundred time intervals between 0 and 3 ps were chosen and the scheme described above was used to obtain the solution as a function of time.

IV. RESULTS AND DISCUSSION

Figure 1 shows the calculated EEDF for various times between 0 and 3 ps. Note that the 0-ps EEDF is spiked at 5 keV and corresponds to the initial conditions discussed above. At first, the EEDF broadens very quickly around 5 keV and starts building up a small low-energy component. As time increases the low-energy component gets larger and the beamlike component around 5 keV gets smaller. At early times, less than a few tenths of a picosecond, low-energy electrons of a few hundred eV are produced mainly by ionization by fast electrons that impart little energy to the formerly bound electrons. The broadening of the 5-keV peak is mostly due to electron-electron collisions. By 0.5 ps there is no noticeable bump at 5 keV and the EEDF takes on a familiar Maxwellian form. However, Fig. 2 shows that even at 1.5 ps an underdeveloped low-energy component and a high-energy tail persist. By 3 ps the tail is gone and the EEDF is completely Maxwellian.

Figure 3 shows the corresponding charge state distribution as a function of time. The calculated mean ion charge at 3 ps is 15.4 which corresponds to a free-electron density of 9.2×10^{21} cm^{-3}. The calculated EEDF at 3 ps corresponds to an electron temperature near 1400 eV. Of course, the equilibrium temperature depends on the initial EEDF. Also note that the calculated EEDF and corresponding temperatures include the radiative energy loss. That is, the energy of electron-

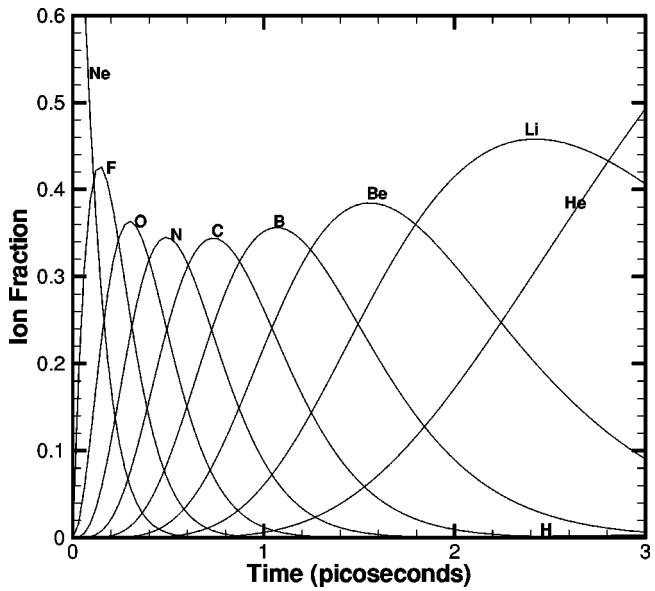

FIG. 3. The calculated ion fractions as a function of time (ps).

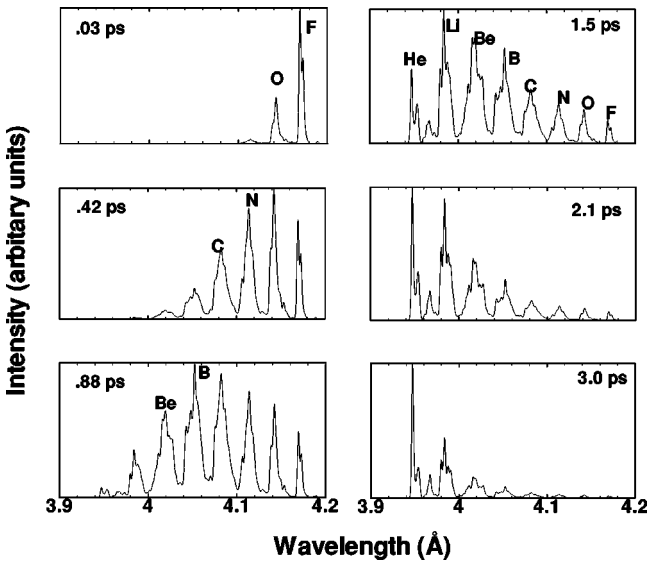

FIG. 4. The calculated time-integrated He_α spectra (arbitrary units) as a function of wavelength (Å) at various times from 0 to 3 ps.

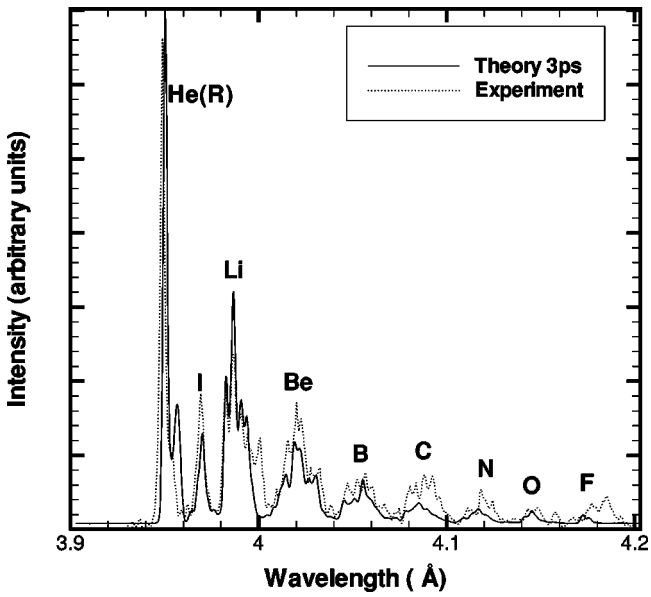

FIG. 5. Comparison of the calculated time-integrated He_α spectrum (solid line) and experiment (dotted line) as a function of wavelength (Å).

impact excitation or ionization followed by radiative decay of the ion is automatically a loss in the total energy of the system. The ionization rate is slower for lower ion densities, and more rapid for higher ion densities using the same initial EEDF.

The time scale for thermalization calculated here is in general agreement with some previous calculations of electron-electron relaxation times [45–47]. The Spitzer [48] self-relaxation time is estimated to be a few tenths of a picosecond, and the actual equilibration times for the EEDF are substantially longer [46]. Note that these authors did not include excitation and ionization in their calculations, which can produce significant differences in the EEDF, by producing low-energy electrons at early times and by introducing energy losses. These authors also did not use the same initial EEDF.

Figure 4 shows the calculated time-integrated emission spectra in the wavelength range near the He_α line and its corresponding satellites for various times from 0 to 3 ps. The emission corresponds to $2p$-$1s$ radiative transitions produced by electron-impact excitation and ionization of *K*-shell electrons in the F-like through He-like ion stages of argon. At early times the calculated spectra predicts emission mainly from the F-like and O-like ions indicative of slight ionization from the imposed Ne-like initial condition. As time increases the spectrum shows contributions from the more highly charged ions as they populate in sequence, see Fig. 3, due to electron-impact ionization. The ionization of the *L*-shell ions is rapid through 1.5 ps, see Fig. 3, and emission from all the ion charge states, F-like through He-like is evident. From 1.5–3 ps the ionization slows down due to the higher ionization potential of the He-like ion, so the main effect on the spectrum is to increase intensity of the He-like emission with respect to the Li-like through F-like satellites. In this time span, the EEDF is also approaching a Maxwellian form, see Fig. 1.

Figure 5 shows a comparison of the calculated time-integrated spectra to 3 ps compared to the experimental measurement. The experimental spectrum was obtained with a peak intensity of 1.3×10^{19} W/cm^3 and a 30-fs duration [29]. The agreement with experiment for the He-like to Be-like emission is quite good. Note that the experimental spectral line occurring near 4 Å is spurious and corresponds to He_γ radiation from a different order of crystal reflection. Also note that for Li-like to B-like, the fine details of the calculated spectra within an ion stage, including relative line positions and intensities are in remarkable agreement with experiment. However, the calculated relative intensities of the lower charged ions, C-like to F-like are somewhat low. Some possible explanations are the following: (1) the atomic model used did not include doubly excited states, hence there was no dielectronic recombination, which would have slowed down the ionization rate and increased the emission intensity, (2) emission from less dense plasma, formed from smaller clusters, that ionize less rapidly and contribute more to the measured spectrum for the lower charged ions, (3) radiation from other orders of crystal reflection, (4) emission from the recombining cooling plasma, and (5) inaccuracy of the initial EEDF by leaving out superhot electrons.

Figure 6 shows the development of the He_β line and Li-like satellites for various times to 3 ps. The relative intensity of the He_β line compared to its satellites is proportional to the ratio of the populations of the He-like to Li-like ions. Figure 5 agrees with Fig. 4 for the α spectrum in that the He-like line dominates at 2.1 ps. No progression through F-like through Be-like charge state is apparent, probably because it is much more likely to fill the *K*-shell hole with and *L*-shell electron than an *M*-shell electron in these ions due to population and transition rate considerations. Figure 7 is a comparison of the calculated 3-ps spectra with the measure-

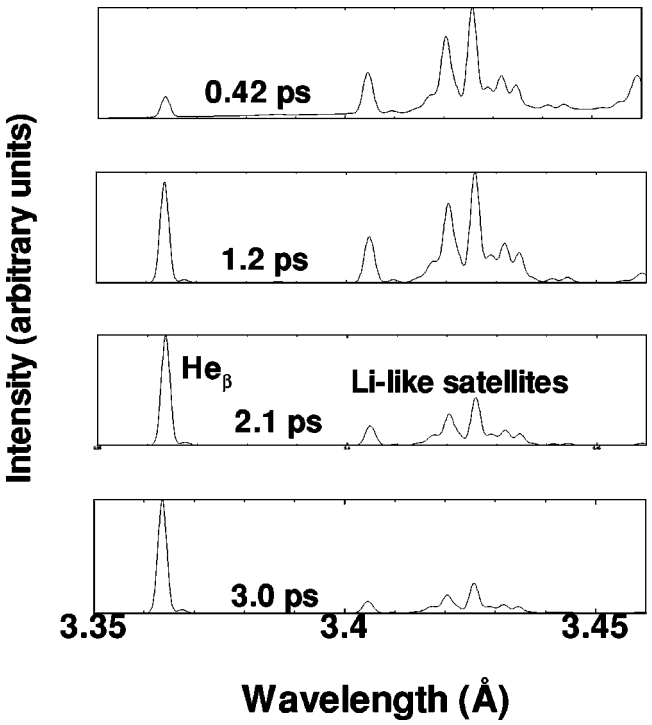

FIG. 6. The calculated time-integrated He_β spectrum (arbitrary units) as a function of wavelength (Å) at various times from 0 to 3 ps.

ment. The results are in good agreement and consistent with the α spectrum, Fig. 5.

The time scale for decay of a cluster, that is expansion and cooling, under the current conditions, has been estimated [49] to be in the range of 1–10 ps. This fact suggests the following scenario for understanding the observed spectra. The main pulse of the laser energy is deposited into the pre-

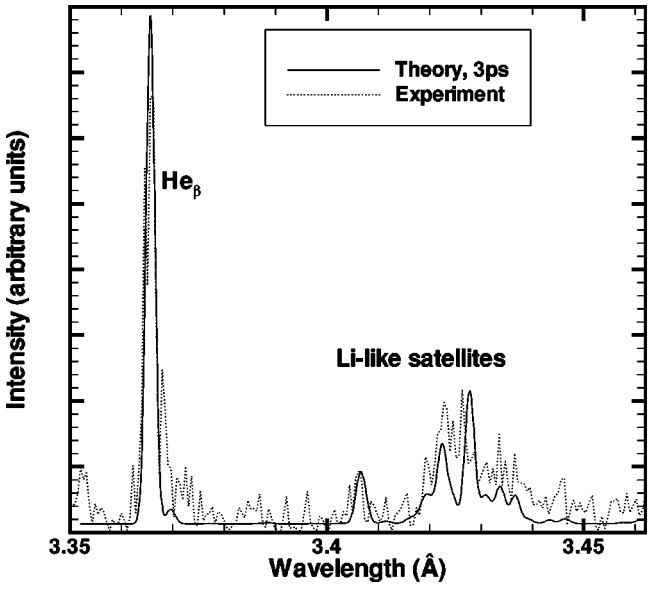

FIG. 7. Comparison of the calculated time-integrated He_β spectrum (solid line) and experiment (dotted) as a function of wavelength (Å).

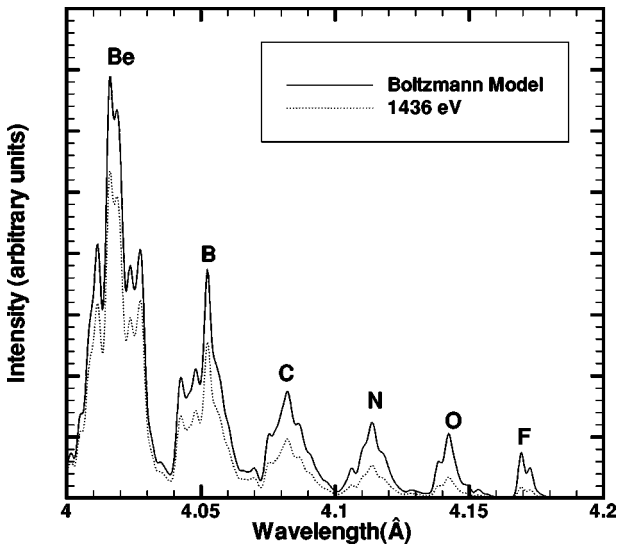

FIG. 8. Comparison of the calculated time-integrated spectra using the Boltzmann model (solid line) and using a constant temperature $kT=1436$ eV (dotted line) at 3 ps as a function of wavelength (Å).

plasma on a femtosecond time scale producing energetic electrons. The relaxation of the hot electrons in the presence of the ions causes excitation and ionization and produces the spectrum discussed above. After a few picoseconds the ionization slows down as the plasma approaches the He-like ionization state and the EEDF approaches a Maxwellian. The expansion and cooling of the cluster then prevent further ionization. It is interesting to note that a previous model [25] with an EEDF involving a static bulk temperature and hot-electron component could not predict either the features of the observed spectra or the expected time scales.

It is interesting to compare the spectra of the Boltzmann model discussed above with a time-dependent model that uses a constant temperature corresponding to the Maxwellian calculated at 3 ps, i.e., $kT=1436$ eV, using the same initial conditions. Figure 8 shows a comparison of the two calculated spectra in the vicinity of the Be-like to F-like satellites. The figure shows that the Be-like to F-like lines are intensified due to the presence of energetic electrons at early times in the Boltzmann model. The He-like and Li-like emission (not shown) are quite similar but slightly less intense for the $kT=1436$-eV case due to the lack of a high-energy tail. The Boltzmann model is an improvement over the constant-temperature model because the intensity of the satellite lines are larger, as observed in the experiment. This result suggests that the inclusion of even more highly energetic electrons, much greater than 5 keV, may also further enhance the emission from these ions.

It is also interesting to compare the Li-like and Be-like satellite line structure for different models because of their sensitivity to dielectronic recombination and inner-shell excitation. Figure 9(a) shows the three groups Li-like spectral lines, qr, a-d, and jkl. The lines qr and a-d are populated mainly by inner-shell excitation from lower levels whose cross sections are large. On the other hand, jkl is mainly populated by dielectronic recombination from the He-like

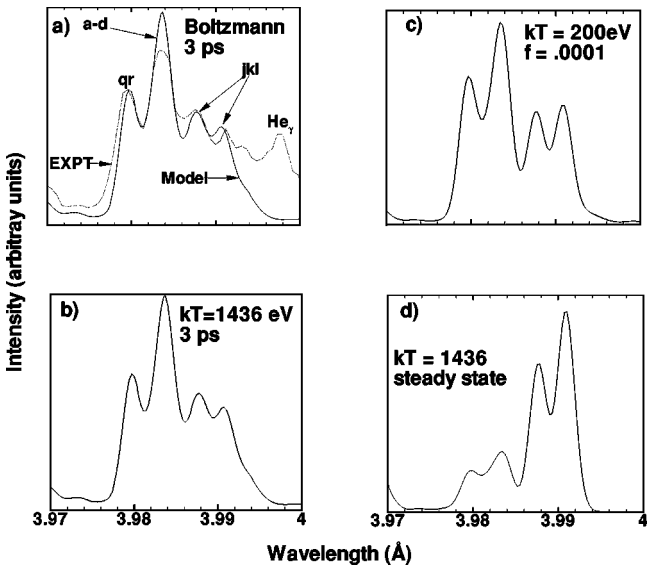

FIG. 9. Comparison of Li-like line structure for (a) the Boltzmann model at 3 ps and experiment; (b) the constant-temperature, $kT=1436$ eV, model at 3 ps; (c) steady state with $kT=200$ and hot-electron fraction f of 0.0001; and (d) steady state at 1436 eV, as a function of wavelength (Å).

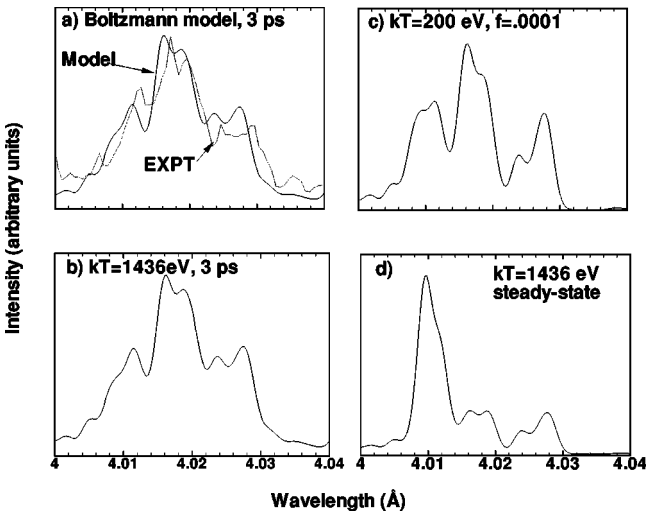

FIG. 10. Comparison of Be-like line structure for (a) the Boltzmann model at 3 ps and experiment; (b) the constant-temperature, $kT=1436$ eV, model at 3 ps; (c) steady state with $kT=200$ and hot-electron fraction f of 0.0001; and (d) steady state at 1436 eV, as a function of wavelength (Å).

ion. For most stationary conditions the relative intensity of jkl is greater than qr or a-d, except when the electron density is very high where electron excitation processes are more dominant. Such electron densities are well beyond those encountered in the present work. It also has been shown [10] that including at hot nonthermal component to a Maxwellian EEDF in a stationary calculation will also intensify qr and a-d with respect to jkl.

Figures 9(a) and 9(b) show the Boltzmann model and the time-dependent constant $kT=1436$ eV model. It is not surprising that the two models give similar results since the Boltzmann model approaches a Maxwellian of 1436 eV at times greater than a few picoseconds without much deviation from Maxwellian form. However, it is interesting that both models predict intense qr and a-d satellite lines without some special prescription for hot electrons. The relative intensities of the Li-like lines calculated here is apparently a high-temperature transient effect, rather than a hot-electron effect, which occurs while the plasma is ionizing. The similarity of Figs. 9(a) and 9(b) show that the transient calculation with the Maxwellian EEDF [Fig. 9(b)], without a hot-electron component, can account for such a satellite structure. Figure 9(a) shows that the calculated relative intensities provide a good fit to the experiment. Note the spurious He$_\gamma$ from the fifth order of crystal reflection which should be ignored. Figure 9(c) shows that a stationary calculation including a hot-electron component with very different plasma parameters, $kT=200$ eV and hot-electron fraction (f) of 0.0001, gives very similar results. Thus, care must be exercised when these methods are used to interpret experimental spectra. Figure 9(d) shows the steady-state calculation corresponding to $kT=1436$ eV, showing the usual domination by the jkl line and demonstrating the transient nature of the Fig. 9(b) case. Note that Figs. 9(a–d) are on different scales to illustrate relative line intensities and the theoretical curve in Fig. 9(a) was scaled to best fit the experimental Li-like line structure.

Figure 10 is similar to Fig. 9 except for the Be-like satellites. Figures 10(a) and 10(b) are similar, again indicative that a Maxwellian EEDF without a hot-electron component in a transient calculation can account for the observed satellite structure shown in Fig. 10(a), which is in excellent agreement with experiment. Figure 10(c) shows that a stationary calculation including a hot-electron component gives similar results, but does not agree with the observations as well as Figs. 10(a) and 10(b). Figure 10(d) shows the steady-state calculation corresponding to $kT=1436$ eV, demonstrating the transient nature of Fig. 10(b) case. However, at $kT=1436$ eV and steady state the Be-like satellites are orders of magnitude weaker than the He-like resonance line and do not contribute noticeably to the overall calculated spectra. Again, Figs. 10(a)–10(d) are on different scales for illustrative purposes.

V. CONCLUSIONS

In summary, a time-dependent plasma kinetics model was used to simulate the time-integrated spectra obtained from ultrafast laser irradiation of argon cluster targets. The model uses the simultaneous solution of the Boltzmann equation for the electron energy distribution function and the rate equations to obtain the populations used in the spectral calculations. The initial EEDF was assumed to be a monoenergetic distribution of energetic (5 keV) electrons, to represent the result of the femtosecond laser pulse energy deposition. Initially, all the ions were assumed to be in the ground state of

the Ne-like ion. The time-integrated spectra calculated to 3 ps is in good agreement with experiment in the wavelength regions near both the He_α and He_β lines. The Boltzmann model predicts the appearance of He-like to F-like x-ray emission that is observed in the experiment. The calculated time scale for emission is also consistent with estimates of cluster decay times for these conditions. The calculations also show that the typical Li-like and Be-like satellite structure, sometimes attributed to a hot-electron component in the EEDF, can also be due to transient effects in a high-temperature ionizing plasma. We hope to use a more realistic initial EEDF in future work.

ACKNOWLEDGMENTS

This work was supported under the auspices of the U.S. Department of Energy at Los Alamos National Laboratory under Contract No. W-7405-ENG-36. The work was also supported in part by the Russian Foundation for Basic Researches (Grant No. 02-01-00708), INTAS (Grant No. 01-0233), and by Grant No. RP1-2328-ME-02 of the U.S. Civilian Research and Development Foundation for the Independent States of the Former Soviet Union (CRDF). The authors thank David P. Kilcrease for valuable discussions and suggestions.

[1] A. McPherson, T.S. Luk, B.D. Thompson, A.B. Borisov, O.B. Shiryaev, X. Chen, K. Boyer, and C.K. Rhodes, Phys. Rev. Lett. **72**, 1810 (1994).

[2] T. Ditmire, T. Donnelly, A.M. Rubenchik, R.W. Falcone, and M.D. Perry, Phys. Rev. A **53**, 3379 (1996).

[3] S. Dobosz, M. Schmidt, M. Perdrix, P. Meynadier, O. Gobert, D. Normand, A.Y. Faenov, A.I. Magunov, T.A. Pikuz, I.Y. Skobelev, and N.E. Andreev, JETP Lett. **68**, 454 (1998).

[4] T. Ditmire, J. Zweiback, V.P. Yanovsky, T.E. Cowan, G. Hays, and K.B. Wharton, Nature (London) **398**, 489 (1999).

[5] S. Dobosz, M. Schmidt, M. Perdrix, P. Meynadier, O. Gobert, D. Normand, K. Ellert, T. Blenski, A.Y. Faenov, A.I. Magunov, T.A. Pikuz, I.Y. Skobelev, and N.E. Andreev, JETP **88**, 1122 (1999).

[6] E. Parra, I. Alexeev, J. Fan, K.Y. Kim, S.J. McNaught, and H.M. Milchberg, Phys. Rev. E **62**, 5931 (2000).

[7] E. Springate, N. Hay, J.W.G. Tisch, M.B. Mason, T. Ditmire, J.P. Marangos, and M.H.R. Hutchinson, Phys. Rev. A **61**, 044101 (2000).

[8] E. Springate, N. Hay, J.W.G. Tisch, M.B. Mason, T. Ditmire, M.H.R. Hutchinson, and J.P. Marangos, Phys. Rev. A **61**, 063201 (2000).

[9] K. Ishikawa and T. Blenski, Phys. Rev. A **62**, 063204 (2000).

[10] J. Abdallah, Jr., A.Y. Faenov, I.Y. Skobelev, A.I. Magunov, T.A. Pikuz, T. Auguste, P. D'Oliveira, S. Hulin, and P. Monot, Phys. Rev. A **63**, 032706 (2001).

[11] G.C. Junkel-Vives, J. Abdallah, Jr., F. Blasco, C. Stenz, F. Salin, A. Ya Faenov, A.I. Magunov, T.A. Pikuz, and I. Yu Skobelev, Phys. Rev. A **64**, 021201R (2001).

[12] G.C. Junkel-Vives, J. Abdallah, Jr., F. Blasco, C. Stenz, F. Salin, A. Ya Faenov, A.I. Magunov, T.A. Pikuz, I. Yu Skobelev, T. Auguste, P.D. Oliveira, S. Hulin, P. Monot, and S. Dobosz, J. Quant. Spectrosc. Radiat. Transf. **71**, 417 (2001).

[13] A.I. Magunov, T.A. Pikuz, I.Yu. Skobelev, A. Ya Faenov, F. Blasco, F. Dorchies, T. Caillaud, C. Bonte, F. Salin, C. Stenz, P.A. Loboda, I.A. Litvinenko, V.V. Popova, G.V. Baidin, G.C. Junkel-Vives, and J. Abdallah, Jr., JETP Lett. **74**, 375 (2001).

[14] H.M. Milchberg, S.J. McNaught, and E. Parra, Phys. Rev. E **64**, 056402 (2001).

[15] E.A. Chowdhury, C.P.J. Barty, and B.C. Walker, Phys. Rev. A **63**, 042712 (2001).

[16] T.D. Donnelly, M. Rust, I. Weiner, M. Allen, R.A. Smith, C.A. Steinke, S. Wilks, J. Zweiback, T.E. Cowan, and T. Ditmire, J. Phys. B **34**, L313 (2001).

[17] L.M. Chen, J.J. Park, K.-H. Hong, J.L. Kim, J. Zhang, and C.H. Nam, Phys. Rev. E **66**, 025402R (2002).

[18] G.C. Junkel-Vives, J. Abdallah, Jr., T. Auguste, P. D'Oliveira, S. Hulin, P. Monot, S. Dobosz, A.Y. Faenov, A.I. Magunov, T.A. Pikuz, I.Y. Skobelev, A.S. Boldarev, and V.A. Gasilov, Phys. Rev. E **65**, 036410 (2002).

[19] G.C. Junkel-Vives, J. Abdallah, Jr., F. Blasco, C. Stenz, F. Salin, A. Y Faenov, A.I. Magunov, T.A. Pikuz, and I.Y. Skobelev, Phys. Rev. A **66**, 033204 (2002).

[20] S.B. Hansen, A.S. Shlyaptseva, A.Y. Faenov, I.Y. Skobelev, A.I. Magunov, T.A. Pikuz, F. Blasco, F. Dorchies, C. Stenz, F. Salin, T. Auguste, S. Dobosz, P. Monot, P. D' Oliveira, S. Hulin, U.I. Safronova, and K.B. Fournier, Phys. Rev. E **66**, 46412 (2002).

[21] I.Yu. Skobelev, A.Y. Faenov, A.I. Magunov, T.A. Pikuz, A.S. Boldarev, V.A. Gasilov, J. Abdallach, Jr., G.C. Junkel-Vives, T. Auguste, P. D'Oliveira, S. Hulin, P. Monot, F. Blasco, F. Dorchies, T. Caillaud, C. Bonte, C. Stenz, F. Salin, and B.Y. Sharkov, JETP **94**, 73 (2002).

[22] I.Y. Skobelev, A.Y. Faenov, A.I. Magunov, T.A. Pikuz, A.S. Boldarev, V.A. Gasilov, J. Abdallah, Jr., G.C. Junkel-Vives, T. Auguste, S. Dobosz, P. D'Oliveira, S. Hulin, P. Monot, F. Blasco, F. Dorchies, T. Caillaud, C. Bonte, C. Stenz, F. Salin, P.A. Loboda, I.A. Litvinko, V.V. Popova, G.V. Baidin, and B.Yu. Sharkov, JETP **94**, 966 (2002).

[23] A.I. Magunov, A.Y. Faenov, I.Y. Skobelev, T.A. Pikuz, E. Bimont, P. Quinet, F. Blasco, C. Bonte, F. Dorchies, T. Caillaud, F. Salin, and C. Stenz, JETP **95**, 998 (2002).

[24] Y. Kishimoto, T. Masaki, and T. Tajima, Phys. Plasmas **9**, 589 (2002).

[25] J. Abdallah, Jr., G.C. Junkel-Vives, A.Y. Faenov, I.Y. Skobelev, T.A. Pikuz, A.I. Magunov, F. Blasco, C. Bonte, F. Dorchies, T. Caillaud, F. Salin, and C. Stenz, J. Quant. Spectrosc. Radiat. Transf. **81**, 3 (2003).

[26] K.Y. Kim, I. Alexeev, E. Parra, and H.M. Milcheberg, Phys. Rev. Lett. **90**, 023401 (2003).

[27] M.B. Smirnov and V.P. Krainov, Phys. Plasmas **10**, 443 (2003).

[28] I. Alexeev, T.M. Antonsen, K.Y. Kim, and H.M. Milchberg, Phys. Rev. Lett. **90**, 103402 (2003).

[29] Y. Fukuda, Y. Akahane, M. Aoyama, N. Inoue, H. Ueda, K. Yamakawa, J. Abdallah, Jr., G. Csanak, A.Y. Faenov, A.I. Ma-

gunov, T.A. Pikuz, I.Y. Skobelev, A.S. Boldarev, and V.A. Gasilov, JETP Lett. (to be published).
[30] J. Zweiback, T.E. Cowan, R.A. Smith, J.H. Hartley, R. Howell, C.A. Steinke, G. Hays, K.B. Wharton, J.K. Crane, and T. Ditmire, Phys. Rev. Lett. **85**, 3640 (2000).
[31] G. Grillon, Ph. Balcou, J.-P. Chambaret, D. Hulin, J. Martino, S. Moustaizis, L. Notebaert, M. Pittman, Th. Pussieux, A. Rousse, J-Ph. Rousseau, S. Sebban, O. Sublemontier, and M. Schmidt, Phys. Rev. Lett. **89**, 065005 (2002).
[32] K. Yamakawa, M. Aoyama, S. Matsuoka, T. Kase, Y. Akahane, and H. Takuma, Opt. Lett. **23**, 1468 (1998).
[33] K. Yamakawa and C.P.J. Barty, IEEE J. Sel. Top. Quantum Electron. **6**, 658 (2000).
[34] A.S. Boldarev, V.A. Gasilov, F. Blasco, C. Stenz, F. Dorchies, F. Salin, A.Y. Faenov, T.A. Pikuz, A.I. Magunov, and I.Y. Skobelev, JETP Lett. **73**, 514 (2001).
[35] A. S. Boldarev, V. A. Gasilov, and A. Y. Faenov (unpublished).
[36] A.Y. Faenov, S.A. Pikuz, A.I. Erko, B.A. Bryunetkin, V.M. Dyakin, G.V. Ivanenkov, A.R. Mingaleev, T.A. Pikuz, V.M. Romanova, and T.A. Shelkovenko, Phys. Scr. **50**, 333 (1994).
[37] T.A. Pikuz, A.Y. Faenov, S.A. Pikuz, V.M. Romanova, and T.A. Shelkovenko, J. X-Ray Sci. Technol. **5**, 323 (1995).
[38] I.Y. Skobelev, A.Y. Faenov, B.A. Bryunetkin, V.M. Dyakin, T.A. Pikuz, S.A. Pikuz, T.A. Shelkovenko, V.M. Romanova, and A.R. Mingaleev, JETP **81**, 692 (1995).
[39] B.K.F. Young, A.L. Osterheld, D.F. Price, R. Shepherd, R.E. Stewart, A.Y. Faenov, A.I. Magunov, T.A. Pikuz, I.Y. Skobelev, F. Flora, S. Bollanti, P. Di Lazzaro, T. Letardi, A. Grilli, L. Palladino, A. Reale, A. Scafati, and L. Reale, Rev. Sci. Instrum. **69**, 4049 (1998).
[40] J. Bretagne, J. Godart, and V. Puech, J. Phys. D **15**, 2205 (1982).
[41] J. Abdallah, Jr., R.E.H. Clark, D.P. Kilcrease, G. Csanak, and C.J. Fontes, in *Atomic Processes in Plasmas*, edited by Albert L. Osterheld, and William H. Goldstein, AIP Conf. Proc. 381 (AIP, Woodbury, NY, 1996), p. 131.
[42] M.N. Rosenbluth, W.M. MacDonald, and D.L. Judd, Phys. Rev. **107**, 1 (1957).
[43] R.E.H. Clark, J. Abdallah, Jr., and J.B. Mann, Astrophys. J. **381**, 597 (1991).
[44] J. Abdallah, Jr., A.Y. Faenov, M. Scholz, L. Karpinski, S.A. Pikuz, V.M. Romanova, M. Sadowski, and A. Szydlowski, J. Quant. Spectrosc. Radiat. Transf. **62**, 85 (1999).
[45] W.M. MacDonald, M.N. Rosenbluth, and W. Chuck, Phys. Rev. A **107**, 350 (1957).
[46] D.C. Montgomery and D.A. Tidman, *Plasma Kinetic Theory* (McGraw-Hill, New York, 1964).
[47] B.J. Albright, D. Winske, D.S. Lemons, W. Daughton, and M.E.S. Jones, IEEE Trans. Plasma Sci. **31**, 19 (2003).
[48] L. Spitzer, *Physics of Fully Ionized Gases* (Interscience, New York, 1954).
[49] T. Auguste, P. D'Oliveira, S. Hulin, P. Monot, J. Abdallah, Jr., A.Yl. Faenov, I.Y. Skobelev, A.I. Magunov, and T.A. Pikuz, JETP Lett. **72**, 55 (2000).